Supporting Information

Supplementary Analyses and Imaging Methods

1. Correlation-Map Analysis

To supplement the whole-brain contrast analyses and ROI correlation analyses reported in the article, we also conducted exploratory whole-brain correlation analyses involving the estimated criterion parameters from the exemplar model. In these analyses, we computed correlations between the maximum-likelihood values of *K* (considered simultaneously across all three tasks and all subjects) and the old-random BOLD percent signal change at every voxel for all of the tasks. Thus, each individual voxel correlation was computed across 54 pairs of scores. One member of each pair was the maximum-likelihood estimate of *K* for subject *i* in task *j*; the other member was the old-random BOLD percent signal change for subject *i* in task *j* computed at that voxel. Correction for multiple tests was done using the FWE method (described in the article) to determine brain regions whose activity patterns showed significant correlations with the estimated criterion parameters, making the assumption, for simplicity, that all 54 pairs of observations were independent. These *p* values need to be interpreted with caution, because each subject contributes three observations to the computation of the correlation, which likely leads to a more liberal criterion than if there were 54 independent subjects. Thus, these analyses should be viewed as an exploratory, descriptive complement to the main contrast analyses reported in the text, which used a very strict statistical criterion..

The correlation map derived with this method is displayed in Figure SI1. In convergence with the results from the contrast analyses, the map shows strong activation

in FEF and AIC. In the present analyses, this result is revealed as bilateral activation of these regions, whereas in the contrast analyses only unilateral activation of these regions reached the strict statistical threshold. In addition, the correlation map revealed significant activation in the posterior parietal cortex and lateral occipital cortex. Although there were no significant clusters in the parietal or occipital cortex in our contrast analyses using the strict threshold, there were significant clusters with the more lenient threshold and these regions overlapped with the regions found in the present correlation analysis. As noted in our article, there is extensive past evidence to suggest that areas of posterior parietal cortex are associated with evidence accumulation in perceptual decision making (28, 32, SI1-2). Likewise, there is also some past evidence that implicates lateral occipital cortex (32, SI3-4). Finally, the correlation map also showed significant clusters in the head and body of the caudate nucleus, the dorsal ACC, and the dorsolateral prefrontal cortex. None of these regions overlapped with any clusters found in the contrast analysis, even with the lenient threshold. However, all of the clusters described for the correlation analysis have been implicated in accumulation of evidence for categorization or other perceptual decision-making tasks in previous studies (28, 32, 34-35, SI1-2).

2. Region of Interest (ROI) Analysis in Posterior Occipital Cortex (POC)

We conducted an ROI analysis comparing old-random activity levels in the region of POC that had been identified by Reber et al. as giving rise to different activation patterns for categorization versus recognition (Talairach coordinates [12 –93 17]; MNI coordinates [12 -97 13]). The results are shown in Figure SI2. As can be seen in the

figure, despite differences in procedure across the two studies, we observed the same patterns of activity as did Reber et al., with negative activations for categorization but positive activations for recognition. Crucially, however, the same ROI analysis conducted on the brain-imaging data from our lax-recognition condition more closely matches the results from our categorization condition, not the recognition condition – see Figure SI2.

3. Analysis of Order Effects

In one set of analyses, we tested whether the patterns of brain activity in the regions of interest (AIC, FEF, and ACC) differed for the LAX condition depending on whether it was tested before or after the CAT condition. Note that there were nine subjects in the pre-CAT condition and nine subjects in the post-CAT condition. (This mode of analysis ignores the positioning of the REC condition.) For AIC and FEF, the unit of analysis was the old-random BOLD percent signal change, whereas for ACC the unit of analysis was the old+random BOLD percent signal change. The results are displayed in Figure SI3. None of the differences approached statistical significance [($t(16) = 0.27$, $p = .79$ in AIC; $t(16) = 0.41$, $p = .68$ in FEF; $t(16) = 1.21$, $p = .25$ in ACC].

In a second set of analyses, we tested whether the patterns of performance across all three conditions (CAT, LAX, and REC) varied during the experimental session. Recall that each of the tasks was tested twice in two repeated triads (see Methods section of article). The brain-activity results for each task in each repetition are displayed in Figure SI4, with a separate panel for each brain region of interest (AIC, FEF, and ACC). Again, for AIC and FEF, the unit of analysis is the old-random BOLD percent signal

change, whereas for ACC the unit of analysis is the old+random BOLD percent signal change. We analyzed the data in each brain region using a 2 (repetition) by 3 (task) repeated-measures analysis of variance. Of course, the main effect of task was highly significant in all three brain regions, as already revealed by the whole-brain analyses reported in the article [$F(2, 17) = 9.1$, $p = .001$ for AIC; $F(2, 17) = 8.7$, $p = .001$ for FEF; $F(2, 17) = 20.8$, $p = .000$ for ACC]. The important new question is whether or not these patterns of brain activity interacted with repetition. Although there are hints of certain changes from the first to the second repetition, the directions of change are not consistent across the different brain regions. Most important, none of the interaction effects between task and repetition approached statistical significance [$F(2, 17) = 0.87$, $p=.43$ in AIC; $F(2, 17) = 1.40$, $p = .26$ in FEF; $F(2, 17) = 1.98$, $p = .15$ in ACC). A reasonable summary statement is that, averaged across the repetitions, the patterns of brain activity line up for CAT and LAX and differ from REC in AIC and FEF; whereas the patterns of brain activity line up for REC and LAX and differ from CAT in ACC.

4. Imaging and Statistical-Analysis Methods

Imaging. MRI data were acquired using a Siemens Magnetom TIM TRIO 3-Tesla whole-body MRI equipped with a 32-channel phased-array head coil. The field of view was 24 x 24 x 11.6 cm, with an in-plane matrix of 96 x 96 pixels and 33 axial slices per volume (whole brain), creating a voxel size of 2.5 mm x 2.5 mm x 3.5 mm. Images were collected using a gradient echo EPI sequence (TE=30ms, TR=2000ms, flip angle=70 degrees) for BOLD imaging. High-resolution T1-weighted anatomical volumes

were acquired using Turbo-flash 3-D sequence (TI=1100 ms, TE = 3.93 ms, TR = 14.375 ms, flip angle = 12 degrees) with 160 1 mm sagittal slices and an in-plane field of view of 224 x 256 (voxel size = 1 mm^3). Imaging data were pre-processed using the SPM8 toolbox for MATLAB (Wellcome Department of Cognitive Neurology, London; http://www.fil.ion.ucl.ac.uk/spm). Anatomical volumes were normalized to a common stereotactic space (Montreal Neurological Institute). Functional volumes were co-registered to the normalized anatomical volumes and then transformed to the common space using a twelve-parameter affine transformation. Functional data underwent 3-D spatial Gaussian filtering (FWHM 8 mm), slice scan-time correction, and 3-D motion correction. Maximum allowable movement was 1.5 mm for gradual drift throughout a functional run and 1 mm for transient motion "spikes".

Statistical Analysis. Normalized functional volumes were analyzed using a random effects general linear model (GLM) procedure to produce statistical parametric maps (SPM). For each participant, the design matrix included regressors for correct trials for old high distortions, new distortions, and random distortions, as well as a combined "wrong" regressor for all incorrect trials. (In the CAT, REC, and LAX conditions, correct responses were defined as "Yes/Old" responses for old items and "No/New" responses for random items. In addition, for REC, "No/New" responses for new distortions were defined as correct responses, whereas for CAT and LAX, "Yes/Old" responses for new distortions were defined as correct responses). Trials were represented as boxcar functions convolved with a canonical two-gamma hemodynamic response function. In addition to these experimental regressors, the design matrix also included regressors for the 6 movement parameters derived from the motion correction

preprocessing stage and a constant for each condition replication. Contrast images for all participants were entered into second-level random-effects group contrast analyses.

References for Supporting Information

1. Daniel R, et al. (2011) Assessing the neural basis of uncertainty in perceptual category learning through varying levels of distortion. J Cogn Neurosci 23(7):1781-1793.

2. Grinband J, Hirsch J, & Ferrera VP (2006) A neural representation of categorization uncertainty in the human brain. Neuron 49(5):757-763.

3. James TW & Gauthier I (2006) Repetition-induced changes in BOLD response reflect accumulation of neural activity. Human Brain Mapping 27:37-46.

4. Philiastides MG & Sajda P (2007) EEG-informed fMRI reveals spatiotemporal characteristics of perceptual decision making. The Journal of Neuroscience 27(48):13082-13091.

Figure Captions for Supporting Information

Figure SI1. Whole-brain correlation map relating old-random BOLD percent signal change to the maximum-likelihood *K* parameters derived by fitting the exemplar model to each individual subject's data in each individual task condition. Numbers in the bottom left corner of each panel reflect position along the z-axis in the MNI reference. AIC = anterior insular cortex, LOC = lateral occipital cortex, caudate = head and body of the caudate, dlPFC = dorsolateral prefrontal cortex, IPL = inferior parietal lobule, FEF = frontal eye fields, SPL = superior parietal lobule.

Figure SI2. Mean BOLD percent signal change in the posterior occipital cortex (POC) for each task (difference effect for the old versus the random patterns).

Figure SI3. Mean Bold percent signal change in the LAX condition as a function of its order of testing with respect to the CAT condition. The results are shown separately for AIC, FEF, and ACC.

Figure SI4. Mean BOLD percent signal change in the CAT, REC, and LAX conditions as a function of task repetition (first versus second triad of testing). The results are shown separately for AIC, FEF, and ACC.

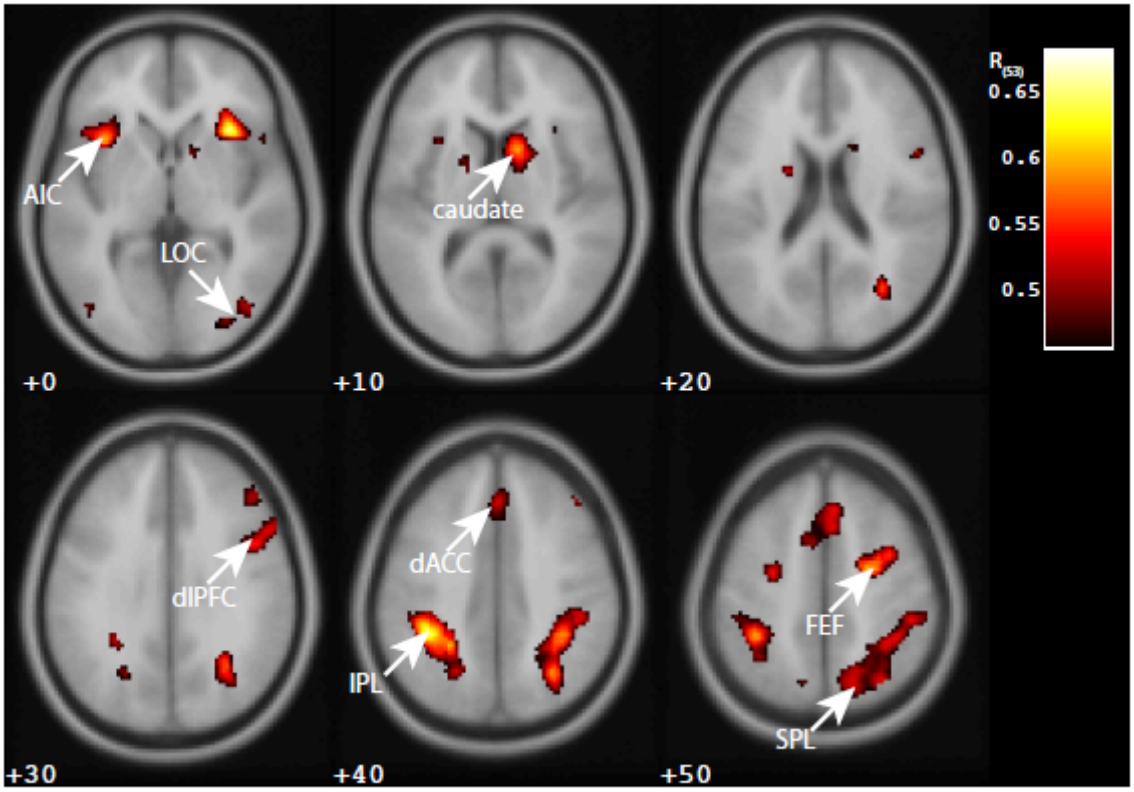
AIC
LOC
caudate
+0
+10
+20
R(53)
0.65
0.6
0.55
0.5
dlPFC
dACC
IPL
FEF
SPL
+30
+40
+50

Figure SI1.

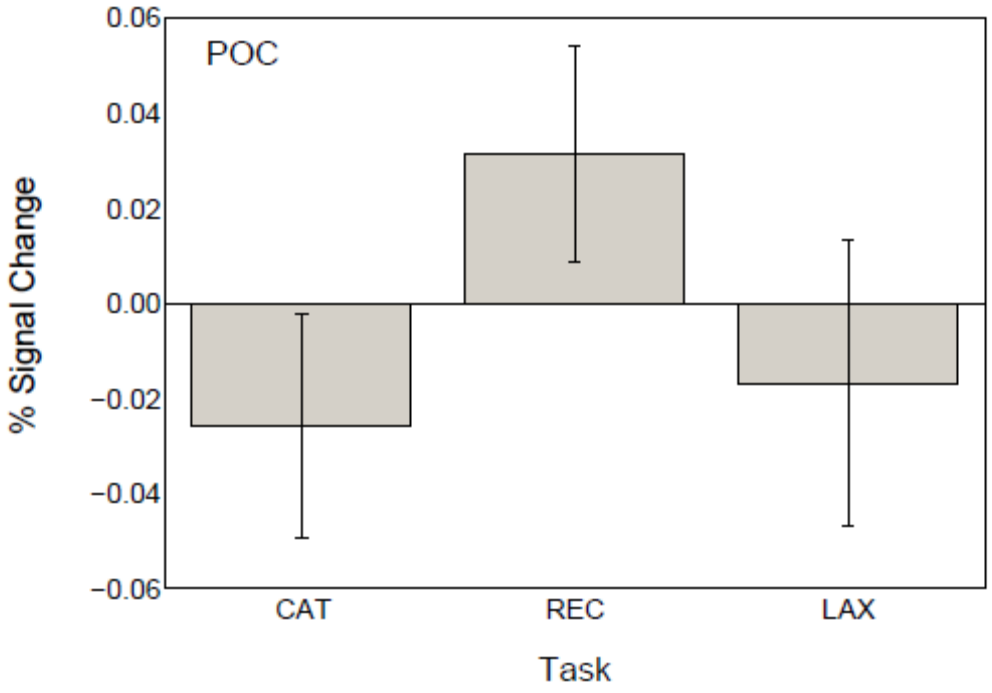

Figure SI2.

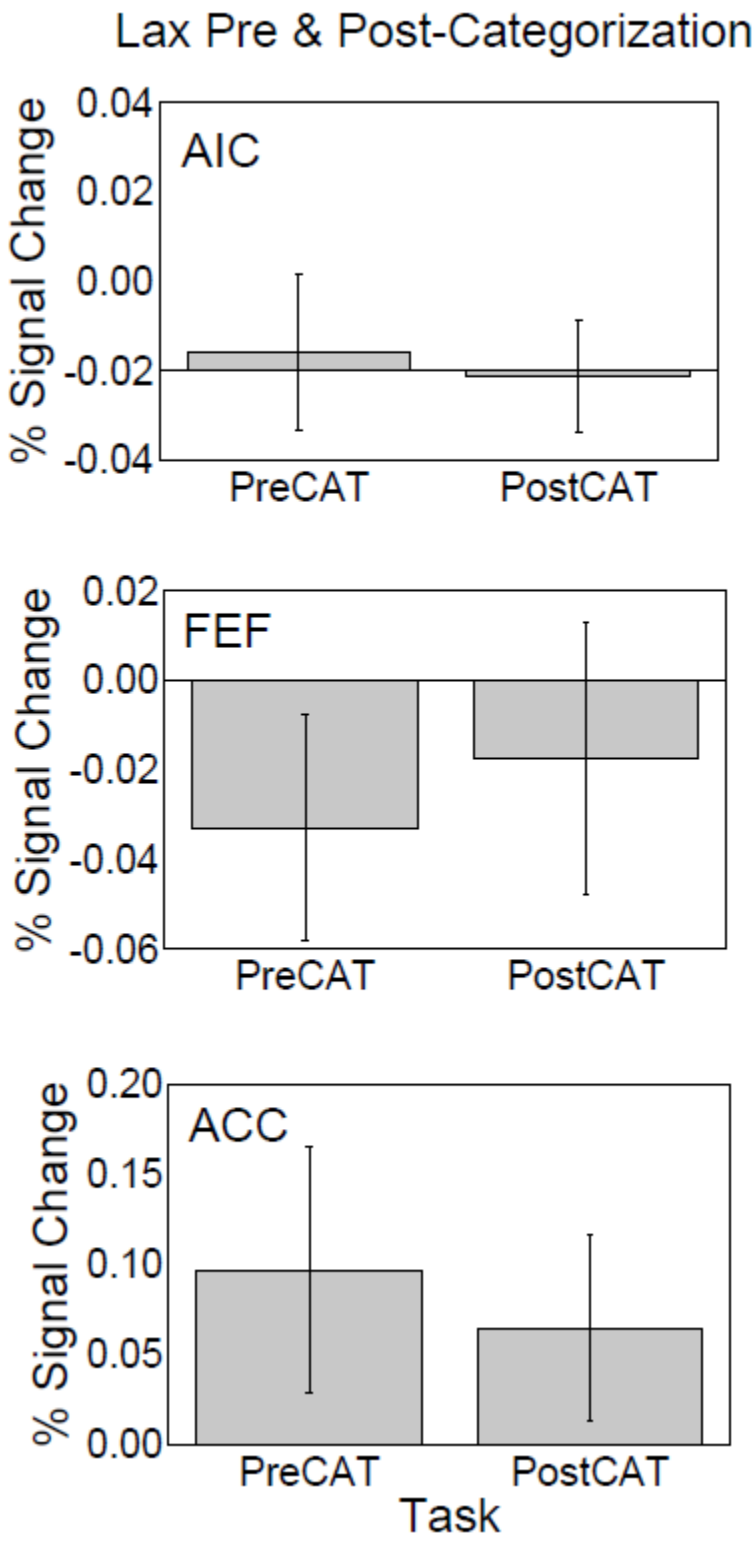
Lax Pre & Post-Categorization
AIC
% Signal Change
0.04
0.02
0.00
-0.02
-0.04
PreCAT
PostCAT
FEF
% Signal Change
0.02
0.00
-0.02
-0.04
-0.06
PreCAT
PostCAT
ACC
% Signal Change
0.20
0.15
0.10
0.05
0.00
PreCAT
PostCAT
Task

Figure SI3.

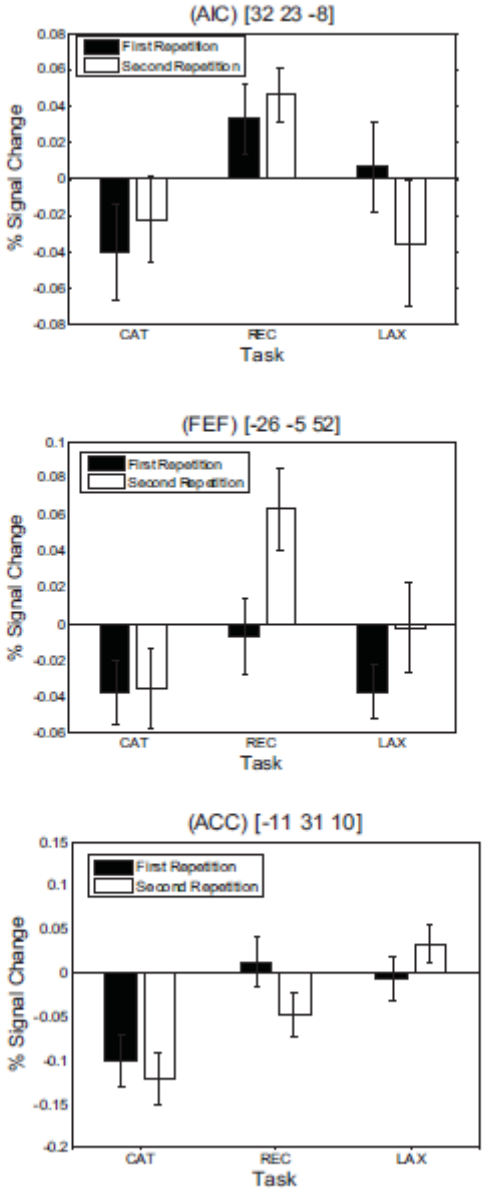
(AIC) [32 23 -8]
First Repetition
Second Repetition
% Signal Change
0.08
0.06
0.04
0.02
0
-0.02
-0.04
-0.06
-0.08
CAT
REC
LAX
Task
(FEF) [-26 -5 52]
First Repetition
Second Repetition
% Signal Change
0.1
0.08
0.06
0.04
0.02
0
-0.02
-0.04
-0.06
CAT
REC
LAX
Task
(ACC) [-11 31 10]
First Repetition
Second Repetition
% Signal Change
0.15
0.1
0.05
0
-0.05
-0.1
-0.15
-0.2
CAT
REC
LAX
Task

Figure SI4.